Phase-field-crystal calculation of crystal-melt surface tension in binary alloys

Nikolas Provatas*
Department of Materials Science and Engineering, McMaster University, 1280 Main Street West, Hamilton, Ontario, Canada L8S 4L7

Sami Majaniemi†
Department of Applied Physics, Aalto University, P.O. Box 11100, FI-00076 AALTO, Finland
(Received 28 July 2010; published 18 October 2010)

A phase field crystal (PFC) density functional for binary mixtures is coarse grained and a formalism for calculating the simultaneous concentration, temperature, and density dependence of the surface energy anisotropy of a solid-liquid interface is developed. The methodology systematically relates bulk free energy coefficients arising from coarse graining to thermodynamic data, while gradient energy coefficients are related to molecular properties. Our coarse-grained formalism is applied to the determination of surface energy anisotropy in two-dimensional Zn-Al films, a situation relevant for quantitative phase field simulations of dendritic solidification in zinc coatings.

DOI: 10.1103/PhysRevE.82.041601 PACS number(s): 81.10.Fq, 81.10.Aj, 68.08.−p, 05.70.Np

I. INTRODUCTION

Multiscale modeling of nonequilibrium phase transformations has seen various advances in recent years. These include very efficient phase field approaches that accurately emulate free-surface models by using diffuse interface widths [1–4] and adaptive mesh refinement techniques for multiscale resolution [5–7]. Recently the phase field methodology has been extended to self-consistently incorporate atomic scale effects, such as elastoplasticity and polycrystalline grain boundary interactions [8–10]. At the heart of this formalism—coined the phase field crystal (PFC) method—is a free energy density that is constructed to be minimized by periodic density states with the symmetries of crystal phases.

Quantitative phase field simulations of microstructure require detailed knowledge of several parameters originating at the microscopic (i.e., atomic) scale. For example, the properties of dendrite solidification depend critically on the crystal-melt surface energy and its anisotropy. Modeling a particular material in a phase field simulation requires that a combination of the model's parameters be matched to its measured surface tension. Unfortunately, in many metallic systems, the surface energy and its anisotropy are not known experimentally, particularly in its temperature and compositional dependence. This problem could be circumvented, in theory, by directly using molecular dynamics or dynamic density functional theory. These methodologies, however, are unable to access the relevant time and length scales of typical phase transformations involved in microstructure evolution.

A compromise in the above problem is to use a static microscopic theory to derive surface energy and some other microscopic parameters that enter higher-scale phenomenological phase field or sharp interface dynamical models. One class of microscopic models for solidification arises from aforementioned classical density functional theory (CDFT) [11]. An even simpler class of atomic scale models are phase field crystal models (PFC) [10], which arise from CDFT by retaining only a crude approximation of the two-point correlation function and reference free energy that enter CDFT. Recent works on pure materials and alloys [12–17] have shown that CDFT models and their PFC simplifications can be scaled up, through different coarse-graining approaches, into complex order parameter models, the latter of which can be further mapped onto traditional phase field models [16].

Toward the above goal, Wu *et al.* [14] recently extended the work of Shih [12] by using classical density functional theory and molecular dynamics to fit the gradient energy coefficients of a phenomenological Ginzburg-Landau model. A prediction of the surface energy of pure iron yielded very good agreement with direct molecular dynamics simulations. Majaniemi and Provatas [16] used coarse graining to obtain a set of complex amplitude equations from a CDFT for a weakly first order transformation in a pure material. Expressions were then derived for the decay length of density waves across the crystal-melt interface, from which surface energy anisotropy was computed.

Encouraged by the success of coarse-graining approaches in pure materials, it is reasonable to expect that extending them to CDFT/PFC type models of multicomponent systems [10] can help elucidate the form of the surface energy and its anisotropy in alloys. This paper applies a coarse-graining procedure to a classical density functional theory of a binary mixture in order to study the temperature and concentration dependence of surface energy. Following Ref. [10], a model of a two-component inhomogeneous fluid is first expressed in terms of two fields; the total atomic number density and the concentration of one of the components. Applying the single-mode approximation used in Ref. [16], a Ginzburg-Landau model is derived in terms of three complex amplitudes (i.e., order parameters), an impurity concentration field and the average density field. This amplitude model is used to predict the surface energy of solid-liquid interface of a binary alloy thin films. The analysis is carried out in two dimensions and applied to thin film Zn-Al coatings, a situation relevant to galvanization of steels.

*provata@mcmaster.ca
†maj@fyslab.hut.fi

II. BINARY ALLOY MODEL

A. Classical density functional theory

The starting point of this work is classical density functional theory [11,18,19], which provides a truncated expansion for the Helmholtz free energy functional of a two component mixture. Written in terms of the atomic number density, $\rho_A(\mathbf{r})$ and $\rho_B(\mathbf{r})$, of species A and B, respectively, this is given by

$$\frac{F}{k_BT} = \int d\mathbf{r}\left\{\rho_A(\mathbf{r})\ln\left(\frac{\rho_A(\mathbf{r})}{\bar{\rho}_A^l}\right) - \delta\rho_A(\mathbf{r}) + \rho_B(\mathbf{r})\ln\left(\frac{\rho_B(\mathbf{r})}{\bar{\rho}_B^l}\right) - \delta\rho_B(\mathbf{r})\right\} - \frac{1}{2}\int\int d\mathbf{r}d\mathbf{r}'\{\delta\rho_A(\mathbf{r})C_{AA}(|\mathbf{r}-\mathbf{r}'|)\delta\rho_A(\mathbf{r}') + \delta\rho_B(\mathbf{r})C_{BB}(|\mathbf{r}-\mathbf{r}'|)\delta\rho_B(\mathbf{r}') + 2\delta\rho_A(\mathbf{r})C_{AB}(|\mathbf{r}-\mathbf{r}'|)\delta\rho_B(\mathbf{r}')\}. \quad (1)$$

The notation $C_{ij}(|\mathbf{r}-\mathbf{r}'|)$ denotes the $i-j$ two-point direct correlation function of a reference liquid phase at temperature $\bar{T}$ in coexistence with a solid. The variable $\bar{\rho}_i^l$ is the average density of the species $i(=A,B)$ in the reference liquid state. For concreteness, coexistence will be characterized by an average density $\bar{\rho}_L \equiv \bar{\rho}_A^l + \bar{\rho}_B^l$ and a temperature T. Finally, $\delta\rho_A \equiv \rho_A(\mathbf{r}) - \bar{\rho}_A^l$ and $\delta\rho_B \equiv \rho_A(\mathbf{r}) - \bar{\rho}_B^l$.

To make contact with traditional thermodynamic and phase field models, it is convenient to work with the transformed fields,

$$\rho(\mathbf{r}) = \rho_A(\mathbf{r}) + \rho_B(\mathbf{r}),$$

$$c(\mathbf{r}) = \frac{\rho_B(\mathbf{r})}{\rho(\mathbf{r})}. \quad (2)$$

The properties of $\rho(\mathbf{r})$ and $c(\mathbf{r})$ can be motivated by writing $\rho_A(\mathbf{r}) \approx n_A(\mathbf{r}) + \Sigma_n A_n e^{i\mathbf{K}^n\cdot\mathbf{r}} + \text{c.c}$ and $\rho_B(\mathbf{r}) \approx n_B(\mathbf{r}) + \Sigma_n B_n e^{i\mathbf{K}^n\cdot\mathbf{r}} + \text{c.c}$, where $\mathbf{K}^n$ are principle reciprocal lattice vectors of the crystal phase and "c.c" denotes the complex conjugate. The fields A_n, B_n are spatially dependent complex amplitudes (units of number density) that become zero in the liquid, while n_A and n_B are spatially varying densities, which attain the respective average value of each component, $\bar{\rho}_A^L$ and $\bar{\rho}_B^L$, in the liquid (which can differ from the average densities of the reference liquid state discussed above). In the solid, the total density $\rho(\mathbf{r})$ oscillates on atomic scales and thus averages, over long enough length scale, to its solid state average, $\rho_s \equiv \bar{\rho}_A^s + \bar{\rho}_B^s$, where $\bar{\rho}_A^s$ and $\bar{\rho}_B^s$ are the values attained by n_A and n_B in the bulk solid phase. The fields A_n, B_n, n_A, and n_B are assumed to vary much more slowly than the phase factors in $\rho_A(\mathbf{r})$ and $\rho_B(\mathbf{r})$. It is also noted that expanding $c(\mathbf{r}) \equiv \rho_B(\mathbf{r})/[\rho_A(\mathbf{r}) + \rho_B(\mathbf{r})]$ [20] to lowest order and coarse graining the gives $\langle c\rangle = \bar{\rho}_B^s/\rho_s \equiv c_s$, the average concentration of component B in the solid.

In terms of the fields $\rho(\mathbf{r})$ and $c(\mathbf{r})$ the free energy in Eq. (1) becomes (relative to a reference state)

$$\frac{\Delta\bar{F}}{k_BT} = \int d\mathbf{r}\left\{\rho\ln\left(\frac{\rho}{\bar{\rho}_L}\right) - \delta\rho + \rho\ln\left(\frac{\bar{\rho}_L}{\bar{\rho}_A^l}\right) + \rho[c\ln c + (1-c)\ln(1-c)] - \rho c\ln\left(\frac{\bar{\rho}_B^l}{\bar{\rho}_A^l}\right) + \rho(1-c)(-1/2C_{BB} - 1/2C_{AA} + C_{AB})(1-c')\rho' + \rho(1-c)(-C_{AB} + C_{BB})\rho' - 1/2\rho C_{BB}\rho' + \rho(1-c)[(-C_{BB} + C_{AB})\bar{\rho}_B^l + (C_{AA} - C_{AB})\bar{\rho}_A^l] + \rho(C_{AB}\bar{\rho}_A^l + C_{BB}\bar{\rho}_B^l)\right\}, \quad (3)$$

where $\rho' \equiv \rho(\mathbf{r}')$ and $c' \equiv c(\mathbf{r}')$ and where correlation operators acting on primed fields (or products of primed fields) denotes integration with respect to $\mathbf{r}'$, i.e., $C_{ij}c'\rho' \equiv \int C_{ij}(|\mathbf{r}-\mathbf{r}'|)c(\mathbf{r}')\rho(\mathbf{r}')d^2\mathbf{r}'$, etc. Unprimed fields are with respect to $\mathbf{r}$. The asymmetry in A and B terms arises due to the definition of c, which assumes B is a minority phase. Equation (3) leads to the alloy PFC model originally developed in Ref. [10] if concentration is defined in terms of A atoms.

B. Coarse grained free energy functional

In this subsection the free energy functional in Eq. (3) is simplified to the level of a phase field crystal (PFC) model by retaining only information of the first peak of the two-point correlation functions. A standard coarse-graining operation is then performed on the resulting free energy functional to project out the long length scales properties in terms of the slow fields A_n, c, and ρ. Following Shih [12], the density $\rho(\mathbf{r})$ is expanded in a *single mode approximation* of the form

$$\rho(\mathbf{r}) = n_0(\mathbf{r}) + \sum_n A_n(\mathbf{r})e^{i\mathbf{K}^n\cdot\mathbf{r}} + \sum_n A_n^*(\mathbf{r})e^{-i\mathbf{K}^n\cdot\mathbf{r}}. \quad (4)$$

The fields $A_n(\mathbf{r})$ and $n_0(\mathbf{r})[\equiv n_A(\mathbf{r}) + n_B(\mathbf{r})]$ are assumed to be slowly varying on scales where $\rho(\mathbf{r})$ varies appreciably. It is similarly assumed that the concentration field $c(\mathbf{r})$ varies slowly on atomic scales, to lowest order in the amplitudes. Finally, the two-point direct correlation functions are expanded in a Fourier series of the form

$$C_{ij}(|\mathbf{r}-\mathbf{r}'|) = \bar{\rho}_L c_{ij}^{\exp}(|\mathbf{r}-\mathbf{r}'|) = \int d\mathbf{k}\hat{C}_{ij}(|\mathbf{k}|)e^{i\mathbf{k}\cdot(\mathbf{r}-\mathbf{r}')}, \quad (5)$$

where i, j denote any of the particle combinations AA, BB, and AB, and "exp" denotes "experimental."

The expansions for $\rho(\mathbf{r})$ and $C_{ij}(|\mathbf{r}-\mathbf{r}'|)$ are substituted into the free energy in Eq. (3), and nonlinear terms are expanded up to fourth order in the fields A_n, n_0 and c. The result is then *coarse grained* according to a box-averaging procedure used in [16]. This integrates out of the free energy contributions arising on atomic scales, which are represented by oscillations of the phase factors in the expansion of $\rho(\mathbf{r})$. Thus, any integral that is a combination of slow fields $[A_n(\mathbf{r}), c(\mathbf{r}),$ and $n_0(\mathbf{r})]$ multiplying phase factors vanishes under coarse graining, unless the phase factor contains a linear combination of the $\mathbf{K}^n$ that sum to zero. This straightforward

albeit lengthy procedure yields a free energy defined on mesoscales written in terms of the slowly varying fields.

The definitions and procedures described in the previous two paragraphs for two-dimensional (2D) HCP symmetry yields the following coarse grained (CG) dimensionless alloy free energy difference in terms of the dimensionless smooth fields $A_m \equiv A_m/\bar{\rho}_L$ $(m=1,2,3)$, $n_0 \equiv n_0/\bar{\rho}_L$ and c,

$$\begin{aligned}\mathcal{F} \equiv \frac{\Delta F_{\mathrm{CG}}}{k_B T \bar{\rho}_L a^2} = \int d\bar{\mathbf{r}} \Bigg\{ & (C^{(1)}c^2 + C^{(2)}c + C^{(3)} + n_0^2 - 3n_0 + 3) \\ & \times (|A_1|^2 + |A_2|^2 + |A_3|^2) + (2n_0 - 3)(A_1 A_2 A_3 + A_1^* A_2^* A_3^*) \\ & + (|A_1|^4 + |A_2|^4 + |A_3|^4)/2 + 2(|A_1|^2|A_2|^2 + |A_1|^2|A_3|^2 \\ & + |A_2|^2|A_3|^2) + [(C_0^{(4)} + \alpha_2)c + C_0^{(5)} + \alpha_1]n_0 + (C_0^{(1)}c^2 \\ & + C_0^{(2)}c + C_0^{(3)} + 3)\frac{n_0^2}{2} - \frac{n_0^3}{2} + \frac{n_0^4}{12} + n_0[c\ \ln(c) + (1 \\ & - c)\ln(1-c)] + \frac{C^{(3)''}}{2}\sum_{m=1}^{3} \mathbf{K}_i^m \mathbf{K}_j^m \frac{\partial A_m^*}{\partial \bar{x}_i}\frac{\partial A_m}{\partial \bar{x}_j} + \frac{\xi_{ij}^{(3)}}{4}\frac{\partial n_0}{\partial \bar{x}_i}\frac{\partial n_0}{\partial \bar{x}_j} \\ & + \frac{C^{(2)''}}{2}\sum_{m=1}^{3} \mathbf{K}_i^m \mathbf{K}_j^m \frac{\partial (cA_m^*)}{\partial \bar{x}_i}\frac{\partial A_m}{\partial \bar{x}_j} + \frac{\xi_{ij}^{(2)}}{4}\frac{\partial (cn_0)}{\partial \bar{x}_i}\frac{\partial n_0}{\partial \bar{x}_j} \\ & + \frac{C^{(1)''}}{2}\sum_{m=1}^{3} \mathbf{K}_i^m \mathbf{K}_j^m \frac{\partial (cA_m^*)}{\partial \bar{x}_i}\frac{\partial (cA_m)}{\partial \bar{x}_j} + \frac{\xi_{ij}^{(1)}}{4}\frac{\partial (cn_0)}{\partial \bar{x}_i}\frac{\partial (cn_0)}{\partial \bar{x}_j} \Bigg\} \end{aligned} \tag{6}$$

Repeated indices (i,j) in Eq. (6) imply summation. Space $(\bar{\mathbf{r}}, \bar{x}_i, \bar{x}_j)$ is in units of the lattice constant "a" and the magnitude of the $\mathbf{K}^m$ is $q_o = 4\pi/\sqrt{3}a$, for a 2D hexagonal crystal. The constants $C^{(N)}$ $(N=1,2,3,4,5)$ are linear combination of the Fourier components $\hat{C}_{ij}(|\mathbf{k}|)$ evaluated at $|\mathbf{k}| = |\mathbf{K}^m| = q_o$. They are given by

$$\begin{aligned} C^{(1)} &= \{2\hat{C}_{AB}(q_o) - [\hat{C}_{AA}(q_o) + \hat{C}_{BB}(q_o)]\}\bar{\rho}_L, \\ C^{(2)} &= 2[\hat{C}_{AA}(q_o) - \hat{C}_{AB}(q_o)]\bar{\rho}_L, \\ C^{(3)} &= -\hat{C}_{AA}(q_o)\bar{\rho}_L, \\ C^{(4)} &= [\hat{C}_{AB}(q_o) - \hat{C}_{AA}(q_o)]\bar{\rho}_L c_o \\ &\quad - [\hat{C}_{AB}(q_o) - \hat{C}_{BB}(q_o)]\bar{\rho}_L(1-c_o), \\ C^{(5)} &= \hat{C}_{AB}(q_o)\bar{\rho}_L(1-c_o) + \hat{C}_{AA}(q_o)\bar{\rho}_L c_o. \end{aligned} \tag{7}$$

The parameters $C_0^{(N)}$ are the same linear combinations of $\hat{C}_{ij}(|\mathbf{k}|)$ as the $C^{(N)}$ but with $|\mathbf{k}|=0$. The constants $C^{(N)''}$ in the gradient terms denote the second derivatives of $C^{(N)}$ with respect to $\mathbf{k}$, then evaluated at $|\mathbf{k}| = |\mathbf{K}^m| = q_o$. The following constants have also been defined:

$$\alpha_1 \equiv \ln\left(1 + \frac{\bar{\rho}_B^l}{\bar{\rho}_A^l}\right) - 11/6 = -\ln(1-c_o) - 11/6,$$

$$\alpha_2 \equiv -\ln\left(\frac{\bar{\rho}_B^l}{\bar{\rho}_A^l}\right) = -\ln\left(\frac{c_o}{1-c_o}\right), \tag{8}$$

where $c_o \equiv \bar{\rho}_B^l/\bar{\rho}_L$ is the average concentration of the reference liquid state. Finally, $\xi_{ij}^{(N)}$ are given by

$$\xi_{ij}^{(N)} = \int \tilde{C}^{(N)}(|\mathbf{R}|) R_i R_j d^2\mathbf{R}, \tag{9}$$

where, for each $N=1,2,3$,

$$\tilde{C}^{(N)}(|\mathbf{R}|) \equiv \mathcal{H}^{-1}\{C^{(N)}(q_o \to |\mathbf{k}|)\}, \tag{10}$$

with $\mathcal{H}^{-1}$ denoting the inverse Fourier transform. The constants in Eqs. (7)–(9) are all generally dependent on temperature through their dependence on the correlation functions at coexistence.

The free energy in Eq. (6) can be made more accurate by considering contributions from higher order direct correlation functions in the expansion of Eq. (1). For example, the $\mathbf{k}=0$ mode of the Fourier representation of the three point correlation function will renormalize the polynomial coefficient of the square amplitude terms [21]. While elegant, a proper inclusion of higher order correlation is a formidable task. In this work, only the *form* of Eq. (6) will be assumed. Bulk free energy coefficients will be fit from thermodynamic database information, while gradient energy coefficients will be inferred from microscopic theories or molecular dynamics.

III. EQUILIBRIUM PROPERTIES OF MODEL

A. Grand potential

The equilibrium fields ρ and c are derived by extremizing the grand potential functional,

$$\begin{aligned} \bar{\Omega} &= F[\rho_A(\rho,c), \rho_B(\rho,c)] - \int d\mathbf{r}\{\mu_A \rho_A(\rho,c) - \mu_B \rho_B(\rho,c)\} \\ &= \bar{F}[\rho,c] - \int d\mathbf{r}\{\mu_A(1-c)\rho - \mu_B c\rho\}, \end{aligned} \tag{11}$$

where $\bar{F}$ is the free energy in Eq. (3), while μ_A and μ_B are the generalized chemical potentials of species A and B, respectively. The definitions of ρ_A and ρ_B in terms of ρ and c have been used in the second line of Eq. (11).

Integrating out the short wavelengths gives the corresponding coarse-grained grand potential $\bar{\Omega}$ in terms of the smooth fields c, n_0, and the A_n. This is given, in dimensionless form, by

$$\Omega = \mathcal{F}[\{A_n\}, c, n_0] - \int [d\bar{\mathbf{r}}\{\mu_A(1-c)n_0 - \mu_B c n_0\}], \tag{12}$$

where, like $\mathcal{F}$ in Eq. (6), Ω is in units of $k_B T \bar{\rho}_L a^2$, while μ_A, μ_B are in units of $k_B T$ and n_0, A_n in units of $\bar{\rho}_L$.

B. Equilibrium profiles

The equilibrium fields $A_n(\mathbf{r})$, $c(\mathbf{r})$, and $n_0(\mathbf{r})$ are found by extremizing Eq. (12) with respect to each A_n, c, and n_0. It

will hereafter be assumed that the complex amplitudes A_n are real. This amounts to writing $A_n=\phi_n e^{\Theta_n(\mathbf{r})}$ in Eq. (6), where ϕ_n is real and $\Theta_n(\mathbf{r})=0$. The amplitudes ϕ_n, c, and n_0 are then given by the solutions of the Euler-Lagrange equations,

$$\frac{\delta\Omega}{\delta\phi_n}=\frac{\delta\mathcal{F}}{\delta\phi_n}=0, \quad n=1,2,3, \tag{13}$$

$$\frac{\delta\Omega}{\delta n_0}=\frac{\delta\mathcal{F}}{\delta n_0}-\mu^{\mathrm{eq}}c-\mu_A^{\mathrm{eq}}=0, \tag{14}$$

$$\frac{\delta\Omega}{\delta c}=\frac{\delta\mathcal{F}}{\delta c}-\mu^{\mathrm{eq}}n_0=0, \tag{15}$$

where $\mu^{\mathrm{eq}}\equiv\mu_B^{\mathrm{eq}}-\mu_A^{\mathrm{B}}$ and where μ_A^{eq} and μ_B^{eq} here denote the dimensionless equilibrium chemical potentials of species A and B, respectively.

To determine surface energy, Eqs. (13)–(15) are solved in one dimension, described here by a dimensionless coordinate $\bar{u}$ which measures distance along the unit normal $\hat{n}$ that defines the orientation of the equilibrium interface under consideration. The explicit form of these one-dimensional (1D) equations is given by Eqs. (A3), (A5), and (A7) in Appendix A.

Equations (A3), (A5), and (A7) are solved subject to boundary conditions, which are established by the bulk equilibrium properties of the free energy of Eq. (6) (where $A_n \rightarrow \phi_n$). Specifically, for a planar solid-liquid interface, Eqs. (A3), (A5), and (A7) must satisfy

$$(c,\rho,\phi_n)\rightarrow(c_L,\rho_L,0) \quad \text{as} \quad \bar{u}\rightarrow\infty,$$

$$(c,\rho,\phi_n)\rightarrow[c_s,\rho_s,\phi_s(c_s,\rho_s)] \quad \text{as} \quad \bar{u}\rightarrow-\infty, \tag{16}$$

where c_s, c_L, ρ_s, and ρ_L denote the equilibrium concentrations and [dimensionless] densities of the bulk solid and liquid phases, and ϕ_s minimizes the bulk solid free energy with respect to ϕ. Appendix B shows how to calculate these boundary conditions.

C. Bulk free energy

The dimensionless bulk free energy is derived from $\mathcal{F}$ in Eq. (6) by making all amplitudes real and equal, i.e., $A_n \rightarrow \phi$, and retaining only the nongradient parts of the free energy density [i.e., integrand of Eq. (6)]. This gives

$$\begin{aligned}\mathcal{G}(\phi,c,n_0)=&\frac{15}{2}\phi^4+(4n_0-6)\phi^3+3(C^{(1)}c^2+C^{(2)}c+C^{(3)}\\&+n_0^2-3n_0+3)\phi^2+\frac{n_0^4}{12}-\frac{n_0^3}{2}+(C_0^{(1)}c^2+C_0^{(2)}c\\&+C_0^{(3)}+3)\frac{n_0^2}{2}+[(C_0^{(4)}+\alpha_2)c+C_0^{(5)}+\alpha_1]n_0\\&+n_0[c\ \ln c+(1-c)\ln(1-c)]\end{aligned} \tag{17}$$

where, here, c, n_0, and ϕ represent the bulk (uniform) values of concentration, density and order parameter in the corresponding solid or liquid phases. (It is recalled that n_0 and ϕ are in units of $\bar{\rho}_L$, and $\mathcal{G}$ in units of $k_BT\bar{\rho}_L$).

1. Specialization to solid and liquid phases

The free energy density $\mathcal{G}$ is specialized to the solid phase by denoting $c=c_s$, $n_0=\rho_s$ and $\phi_s=\beta(c_s,\rho_s)$, where $\beta(c,\rho)$ solves $\partial\mathcal{G}/\partial\phi=0$ for ϕ and is given explicitly by

$$\begin{aligned}\beta(c,\rho)=&\frac{3-2\rho}{10}\\&+\frac{\sqrt{-20(C^{(3)}+C^{(2)}c+C^{(1)}c^2)-51+48\rho-16\rho^2}}{10}\end{aligned} \tag{18}$$

Note that the condition $\beta=0$ defines an maximum concentration [via the radical in Eq. (18)] for which a bulk solid can be defined. The bulk free energy $\mathcal{G}$ is hereafter denoted $\mathcal{G}_s(c_s,\rho_s)$ in the solid.

The free energy $\mathcal{G}$ is specialized to the liquid phase by denoting concentration $c=c_L$ and density $n_0=\rho_L$, and by setting $\phi=0$ ("order" in the liquid is zero). The bulk free energy $\mathcal{G}$ is denoted $\mathcal{G}_L(c_L,\rho_L)$ in the liquid.

2. Determination of bulk coefficients: constant density

This subsection illustrates how to determines the coefficients of $\mathcal{G}_s$ and $\mathcal{G}_L$ by matching the excess (i.e., nonlogarithmic) part of the free energy $\mathcal{G}_s$ and $\mathcal{G}_L$ to the Redlich-Kister form $G_{\mathrm{ex}}^L=G_{L1}c_L+G_{L2}(1-c_L)+\Omega_Lc_L(1-c_L)$, for the liquid, and $G_{\mathrm{ex}}^s=G_{s1}c_s+G_{s2}(1-c_s)+\Omega_sc_s(1-c_s)$ for the solid. The constants G_{Li} and Ω_i $(i=L,s)$ are obtained from the Thermo-Calc database, and are expressed here in units of RT here, where R is the natural gas constant. It is assumed that the solid and liquid densities are equal and equal to $\bar{\rho}_L$. This amounts to setting $\rho_s=\rho_L=1$ in $\mathcal{G}_s$ and $\mathcal{G}_L$ defined in Sec. III C 1.

In the liquid, $\phi=0$ in Eq. (17), and the dimensionless bulk liquid free energy becomes (setting $n_o=1$),

$$\mathcal{G}_L(c_L)=(1-c_L)\ln(1-c_L)+c_L\ln c_L+\frac{B_o^{(1)}}{2}c_L^2+B_o^{(2)}c_L+B_o^{(3)}, \tag{19}$$

where

$$\begin{aligned}B_o^{(1)}&\equiv C_0^{(1)}=-2\Omega_L,\\B_o^{(2)}&\equiv\frac{C_0^{(2)}}{2}+C_0^{(4)}+\alpha_2=G_{L1}-G_{L2}+\Omega_L,\\B_o^{(3)}&\equiv\frac{C_0^{(3)}}{2}+C_0^{(5)}+\alpha1+\frac{13}{12}=G_{L2},\end{aligned} \tag{20}$$

For the bulk solid, the coefficients of the bulk free energy $\mathcal{G}_s$ are obtained by expanding the excess part of $\mathcal{G}_s$ to order $\mathcal{O}(c^2)$ and then matching the result, order by order, to the expansion of G_{ex}^s. This yields

$$\mathcal{G}_s(c_s) = (1-c_s)\ln(1-c_s) + c_s \ln c_s + \left(\frac{B_o^{(1)}}{2} + 3C^{(1)}\phi_s^2\right)c_s^2 + (B_o^{(2)} + 3C^{(2)}\phi_s^2)c_s + [B_o^{(3)} + (15/2)\phi_s^4 - 2\phi_s^3 + 3(C^{(3)}+1)\phi_s^2] \quad (21)$$

where

$$C^{(1)} = -\frac{10}{3}\left\{\frac{10\Omega_s r^{1/2} - Q^3/3 - r^{1/2}Q^2/3 + 5B_o^{(1)}r^{1/2}}{r^{3/2}+2r+r^{1/2}}\right\},$$

$$C^{(2)} \equiv -\frac{Q}{3},$$

$$C^{(3)} \equiv -\frac{r+19}{20}, \quad (22)$$

and where

$$Q = \frac{100r^{1/2}(G_{s2} - G_{s1} - \Omega_s + G_{L1} - G_{L2} + \Omega_L)}{r^{3/2}+2r+r^{1/2}}, \quad (23)$$

while r solves

$$ar^{3/2} + br^2 + cr + (G_{s2} - G_{s1} + 13/12) = 0 \quad (24)$$

(with $a=0.002$, $b=0.00075$ and $c=0.0015$) and $\phi_s \equiv \beta(c=c_s,\ \rho=1) = [1+\sqrt{-20\mathcal{C}_r(c_s)-19}]/10$, where

$$\mathcal{C}_r(c) = C^{(3)} + C^{(2)}c + C^{(1)}c^2 \quad (25)$$

The top frame in Fig. 1 shows the solid and liquid free energies $\mathcal{G}_s(c)$ (blue curve) and $\mathcal{G}_L(c)$ (yellow curve) for Zn-AL at a temperature $T=670$ K. The bottom frame shows the free energy landscape $\mathcal{G}(\phi,c)$ in Eq. (17) from which $\mathcal{G}_s$ and $\mathcal{G}_L$ are extracted (the parameter $n_o=1$). Also shown in the top frame is the Redlich-Kister form of the free energy for each phase. In the case of the liquid, the Redlich-Kister and amplitude model's field free energies overlap identically. For the solid, the amplitude model's free energy (blue curve) overlap the Redlich-Kister only partially. This is because Eq. (17) predicts an order parameter change in the solid [via Eq. (18)] as c increases past the equilibrium concentration c_s; the thermodynamic database prediction is a curve fit based on data acquired experimentally for concentrations near equilibrium, and extrapolated to all concentrations.

D. Surface tension

Let the solutions of Eqs. (A3), (A5), and (A7) across a planar interface be denoted $n_0^*(\bar{u})$, $c^*(\bar{u})$, and $\phi_n^*(\bar{u})$ ($n=1,2,3$). The interface energy is defined as the excess of the grand potential. Its dimensionless form, $\bar{\gamma}$, is by $\bar{\gamma} = \Omega[\phi_n^*(\bar{u}), c^*(\bar{u}), n_0^*(\bar{u})] - \Omega_B$, where Ω_B is the dimensionless grand potential in the bulk solid (or liquid) and $\bar{u}$ is the dimensionless distance along the planar interface [18]. Starting from Eq. (12), Appendixes A and B yield

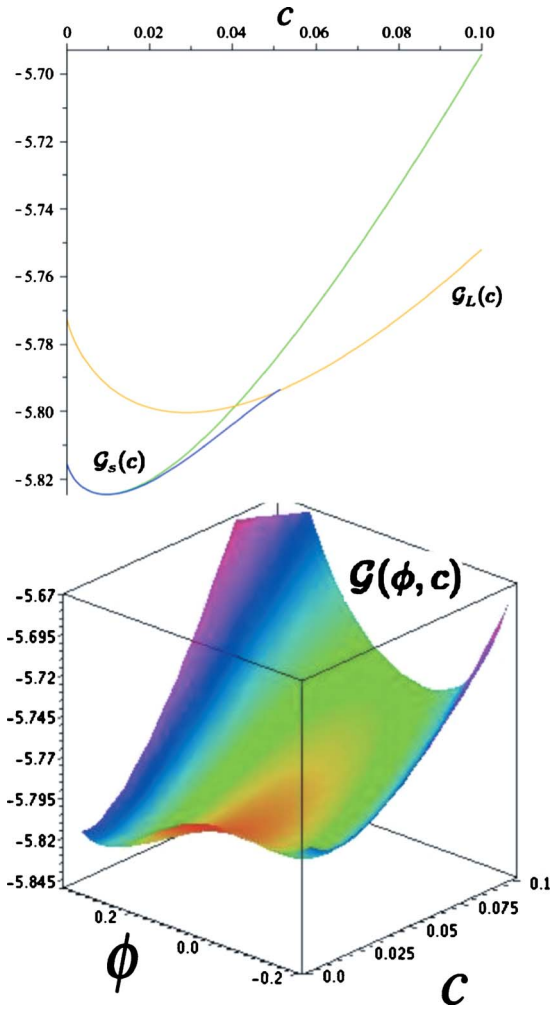

FIG. 1. (Color online) (Top) Phase field free energies of the solid (lowest extending curver—blue) and liquid (nearest to the symbol $\mathcal{G}_L(c)$—yellow). The Redlich-Kister free energies for both phases are superimposed (topmost extending curve—green) for solid, indistinguishable from phase field for liquid. (Bottom) 3D plot of Eq. (17) ($n_o=1$).

$$\bar{\gamma} \equiv \frac{\gamma}{k_B T \bar{\rho}_L a} = \int_{-\infty}^{\infty}\left\{\left[f(\{\phi_n^*\}, c^*, n_0^*) - \frac{n_0^*}{\rho_s}\mathcal{G}_s(c_s,\rho_s)\right] - n_0^*[c^* - c_s]\mu^{\mathrm{eq}} - \left[\frac{n_0^*}{\rho_s} - 1\right]p\right\}d\bar{u} \quad (26)$$

where $f(\{\phi_n\}, c, n_0)$ is the integrand of $\mathcal{F}_{1D}$ in Eq. (A1) [i.e., Eq. (6) for the case of a planar interface], $\mathcal{G}_s(c_s,\rho_s)$ is the bulk solid free energy defined in Sec. III C 1 and p denotes the equilibrium pressure (all in units of $k_B T\bar{\rho}_L$).

IV. CALCULATION OF CRYSTAL-MELT SURFACE TENSION IN ZN-AL FILMS: CONSTANT DENSITY

This section uses the theory of Sec. III to approximate the anisotropic surface energy of a solid-liquid interface for 2D Zn-Al films, where element A denotes Zn and B denotes Al. For simplicity, the approximation of equal density in the

TABLE I. Far-field parameters c_s, c_L, and μ^{eq} used to solve Eqs. (27) and (28). The solid order parameter $\phi_s(c_s)$ is given by Eq. (18).

T (K)	690	684	675	670	662.5
c_s (10^{-2})	0.3067	1.0168	2.0419	2.5803	3.3391
c_l (10^{-2})	0.7824	2.5785	5.3679	6.9732	9.4697
μ_{eq}	−1.3359	−0.1555	0.5570	0.8056	1.0898

solid and liquid phases is assumed. In this limit Eq. (26) reduces to $\bar{\gamma}=\int_{-\infty}^{\infty}\{f(\{\phi_n^*\},c^*)-\mathcal{G}_s(c_s)-[c^*-c_s]\mu^{eq}\}d\bar{u}$, where the density has been set to $n_o=1$ in $f(\{\phi_n\},c,n_0)$ and $\mathcal{G}_s(c_s,\rho_s)$.

The Euler-Lagrange equation for the field ϕ_1^* [Eq. (A3)] reduces at constant density to

$$\frac{(\mathbf{K}^1\cdot\hat{n})^2}{2}\left\{M_{23}(c^*)\frac{\partial^2\phi_1^*}{\partial\bar{u}^2}+M_{12}(c^*)\frac{\partial^2(c^*\phi_1^*)}{\partial\bar{u}^2}\right\}-\{\mathcal{C}_r(c^*)+2(\phi_2^{*2}+\phi_3^{*2})\}\phi_1^*-\phi_1^{*3}+\phi_2^*\phi_3^*=0 \quad (27)$$

where $M_{12}(c)$ and $M_{23}(c)$ are given by Eqs. (A4) and where $\hat{n}$ is the unit normal to the interface. Equations for ϕ_2^* and ϕ_3^* are given by analogous permutations of Eq. (27). The concentration equation [Eq. (A7)] reduces to

$$-\frac{\chi_1(\hat{n})}{2}\frac{\partial^2 c^*}{\partial\bar{u}^2}-\sum_{m=1}^{3}(\mathbf{K}^m\cdot\hat{n})^2\phi_m^*\frac{\partial^2[M_{12}(c^*)\phi_m^*]}{\partial\bar{u}^2}+\ln\left(\frac{c^*}{1-c^*}\right)+(2C^{(1)}c^*+C^{(2)})(\phi_1^{*2}+\phi_2^{*2}+\phi_3^{*2})+B_o^{(1)}c^*+B_o^{(2)}=\mu^{eq}, \quad (28)$$

where χ_1 is given in Eqs. (A2).

Equations (27) and (28) are solved using explicit finite differencing with fictitious time to iterate the equations to their steady state profiles. Boundary conditions for the bulk fields are denoted $c=c_L$ and $\phi_n=0$ as $\bar{u}\to-\infty$ and $c\to c_s$ and $\phi_n=\phi_s(c_s)$ as $\bar{u}\to\infty$. The values of ϕ_s, c_s, c_L, as well as μ^{eq}, are obtained at a given temperature by applying the common tangent construction to the solid and liquid bulk free energies extracted from Eq. (17), the bulk coefficients of which are related to the Redlich-Kister coefficients for each phase as shown in Sec. III C 2. The dimensionless coefficient c_s, c_L, and μ^{eq} are given in Table I for five temperatures.

The gradient coefficients multiplying the order parameter terms of Eqs. (27) and (28) are determined as follows. It is assumed that at coexistence liquid Zn-Al satisfies $\hat{C}''_{AA}(q_o)\approx\hat{C}''_{BB}(q_o)\approx\hat{C}''_{AB}(q_o)$ (A=Zn and B=Al). This gives, $M_{12}=0$ and $M_{23}=C^{(3)''}=-\hat{\rho}_L C''_{AA}(q_o)$. The value of $C''_{AA}(q_o)$ not precisely known for Zn. It is estimated here by comparison with MD simulations for pure Ni at coexistence, where it is found that $\hat{\rho}_L C''_{AA}(q_o)=-10.40$ Å [22]. This is almost identical to the corresponding quantity for iron, where $\hat{\rho}_L C''_{AA}(q_o)=-10.44$ Å [14,15]. Taking $\mathbf{K}^1=q_o(2/\sqrt{3})\hat{j}$, $\mathbf{K}^2=q_o(-\hat{i}-1/\sqrt{3}\hat{j})$, $\mathbf{K}^3=q_o(\hat{i}-1/\sqrt{3}\hat{j})$, and $q_o^{Zn}=2.66$ Å, thus gives $C^{(3)''}(q_o^{Zn})^2=-\hat{\rho}_L C''_{AA}(q_o)(q_o^{Zn})^2\approx 1.1$.

The gradient energy coefficient $\chi_1(\hat{n})$ multiplying the concentration term in Eq. (28) can be shown to be a constant independent of $\hat{n}$, and given by $\chi_1=3\pi\int_0^\infty R^3C^{(1)}(|R|)dR$. Cahn and Hilliard [23] showed this to be given by the coefficient of the enthalpy of mixing term in the free energy of a regular solution. It is thus approximated here by $\Omega_L(T)/RT$ coefficient appearing in the bulk liquid free energy, which was introduced in Sec. III C 2.

The top frame in Fig. 2 plots the surface energy $\bar{\gamma}$ versus the angle θ that the interface normal $\hat{n}$ makes with the x axis. The parameter $\bar{\gamma}_o$ is the isotropic surface energy. Curves for the temperatures T=662.5,670,675,684,690 K are plotted. The data suggest that the two dimensional surface energies can be fit to the form

$$\bar{\gamma}(\theta,T)=\bar{\gamma}_o(T)[1+\epsilon_6(T)\cos(6\theta)], \quad (29)$$

which is a reasonable form, as shown in Ref. [16]. The amplitudes of the different curves represent the surface energy anisotropy, $\epsilon_6(T)$, which is plotted separately, along with $\bar{\gamma}_o(T)$, in Fig. 2. The corresponding stiffness, $\bar{\gamma}(\theta)+\bar{\gamma}'(\theta)$, for each temperature is plotted in Fig. 3. The behavior of $\epsilon_6(T)$ predicted here for an alloy is to be contrasted with the prediction of ϵ_6 for a pure material derived from a Ginzburg-

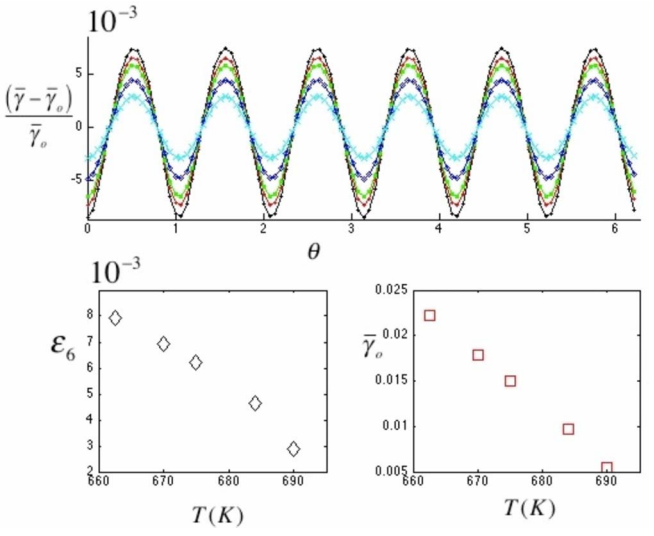

FIG. 2. (Color online) (Top) Normalized crystal-melt surface energy versus angle for different temperature. The lowest amplitude corresponds to the highest temperature (T=690 K), while the highest amplitude to the lowest temperature (T=662.5 K). (Bottom left) Anisotropy parameter ϵ_6 versus temperature. (Bottom right) The isotropic surface energy $\bar{\gamma}_o$ versus temperature.

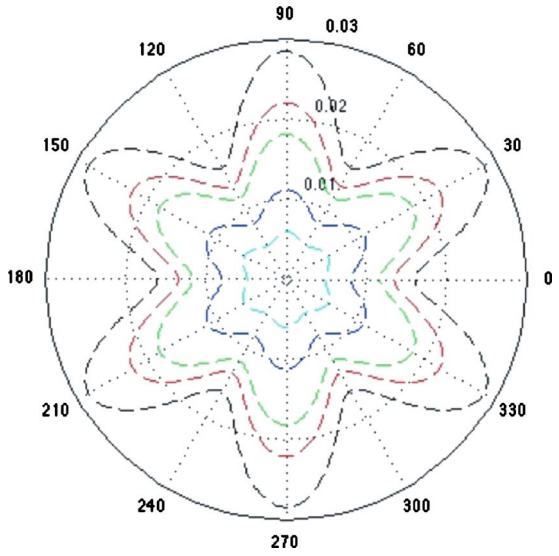

FIG. 3. (Color online) Wulf plots of $\bar{\gamma}(\theta)+\bar{\gamma}'(\theta)$ for the temperatures corresponding to Fig. 2. Inner most curve corresponds to $T=690$ K, while the outer most curve to $T=662.5$ K.

Landau (GL) amplitude model developed in Ref. [16]. In the latter case it was found that ϵ_6 was independent of temperature, at least at the level of a fourth order GL theory.

A 3D calculation of Haxhimali *et al.* [24] recently showed that at least one of the two crystal-melt anisotropy parameters in Zn-Al decreases as the average Zn content increases. This is consistent with the trend of $\epsilon_6(T)$ in Fig. 2, since increasing temperatures increases the range of Zn concentration required for coexistence. The largest value of ϵ_6 in Fig. 2 is also close to the anisotropy in a binary system studied by molecular dynamics by Becker *et al.* [25]. The variation of anisotropy in that work is smaller than that in this work however. This may be due to the small partition coefficient in their alloy system. Amini *et al.* [26] similarly found that a model hard sphere system exhibits a small variation of anisotropy versus temperatures—although their predictions are higher than either our work or that of Becker *et al.* Finally, it is also interesting to note that the range of ϵ_6 in this work overlaps with the anisotropy for pure BCC iron reported in [14], where $\epsilon_4=(\gamma_{100}-\gamma_{110})/(\gamma_{100}+\gamma_{110})\sim 0.5-1\%$.

Experimental work by Passerone *et al.* [27] and Miller *et al.* [28] has shown that the anisotropy in some zinc alloys increases with decreasing temperature, which is consistent with the results of this work. These experimental works they also show that well below the melting point some zinc alloys can exhibit a transition to faceted interfaces. Ising type models with short range interactions have shown that a roughening transition exists at a temperature $T>0$ in 3D, but only at $T=0$ in 2D, at least in the mean field sense without thermal noise [29]. As a result, it is expected that one must extend the techniques developed here to 3D in the presence of noise to predict a roughening transition.

V. CONCLUSION

This single mode density wave expansion used here, and the coarse-graining formalism used to arrive at an effective complex amplitude model coupling amplitudes, concentration, and density can easily be extended to three spatial dimensions. The reader is referred to Ref. [21] for an complimentary coarse-graining approach to that used here that shows the details of this procedure. The application of this theory to the determination of surface energy anisotropy in dilute 2D Zn-Al alloys can be directly applicable to quantitative phase field simulations of dendritic solidification of zinc coatings.

It was found that both the isotropic and anisotropic parts of the surface energy ($\bar{\gamma}_{\rm iso}$ and ϵ_6) were dependent on temperature. In this temperature dependence there is buried an implicit concentration dependence due to impurity segregation [$\Delta c(T)=c_L-c_s$], since an analogous model studied recently for a pure material [16] revealed no change in anisotropy parameter as temperature (and average density) changed. It would be useful to explicitly separate out this concentration dependence into the form $\epsilon_6(T) \equiv \bar{\epsilon}_6[T,\Delta c_o(T)]$. This can be accomplished by considering ternary alloy system, where it is possible to change in the concentration of a ternary component in order to induce a corresponding change in the solid-liquid coexistence concentrations of the primary and secondary components *without* changing temperature. This system can be treated as an effective binary in which changes of Δc_o can be induced at constant temperature [30].

As a final comment, it is noted that Eqs. (20) and (22) can in principle be used to relate the properties of the correlation functions $\hat{C}_{AA}$, $\hat{C}_{BB}$, and $\hat{C}_{AB}$, at $|\mathbf{k}|=q_o$ and $|\mathbf{k}|=0$, to the coefficients of the bulk free energies, which are determinable from some thermodynamic database. In the present approximation of equal solid and liquid density, Eqs. (20) and (22) become undetermined, requiring a higher order amplitude, concentration and density expansion of the amplitude model to acquire more equations. However, since only the form of the free energy was considered in this work, only groupings of coefficients (i.e., the effective coefficients, $B_o^{(1)}$, $B_o^{(2)}$, $B_o^{(3)}$, $C^{(1)}$, $C^{(2)}$, and $C^{(3)}$) were fit from thermodynamic data.

ACKNOWLEDGMENTS

The authors would like to thank Jeff Hoyt for useful discussions and insight. N.P. acknowledges the National Science and Engineering Research Council of Canada (NSERC) for Funding. S.M. and N.P. acknowledge the Finnish TEKES MASI program for funding.

APPENDIX A: EULER LARGRANGE EQUATIONS

Equations (13)–(15) are written in 1D with respect to a variable $\bar{u}$ transverse to a planar interface defined by the unit normal $\hat{n}$ which is at an angle θ to the x axis (i.e., $\hat{n}\equiv\hat{n}_x\hat{i}+\hat{n}_j\hat{j}=\cos\theta\hat{i}+\sin\theta\hat{j}$). Their explicit form is obtained by extremizing $\mathcal{F}$ with respect to ϕ_n, c and n_0 (i.e., $A_n\rightarrow$ real amplitudes ϕ_n). For the case of a planar interface $\mathcal{F}$ becomes

$$\mathcal{F}_{1D}(\{\phi_n\},c,n_0) = \int_{-\infty}^{\infty} \left[\sum_{i=1}^{3} \left\{ H(c,n_0)\phi_i^2 + \frac{\phi_i^4}{2} + \phi_i^2 \sum_{j\neq i} \phi_j^2 \right\} + 2(2n_0-3)\prod_{i=1}^{3}\phi_i + n_0(c\ln(c) + (1-c)\ln(1-c)) + G_2(c)n_0 + G_3(c)\frac{n_0^2}{2} - \frac{n_0^3}{2} + \frac{n_0^4}{12} + \sum_{m=1}^{3} (\mathbf{K}^m\cdot\hat{n})^2 \left\{ \frac{C^{(3)\prime\prime}}{2}\left(\frac{\partial\phi_m}{\partial\bar{u}}\right)^2 + \frac{C^{(2)\prime\prime}}{2}\frac{\partial\phi_m}{\partial\bar{u}}\frac{\partial(c\phi_m)}{\partial\bar{u}} + \frac{C^{(1)\prime\prime}}{2}\left(\frac{\partial(c\phi_m)}{\partial\bar{u}}\right)^2 \right\} + \frac{\chi_3(\hat{n})}{4}\left(\frac{\partial n_0}{\partial\bar{u}}\right)^2 + \frac{\chi_2(\hat{n})}{4}\frac{\partial(cn_0)}{\partial\bar{u}}\frac{\partial n_0}{\partial\bar{u}} + \frac{\chi_1(\hat{n})}{4}\left(\frac{\partial(cn_0)}{\partial\bar{u}}\right)^2 \right] d\bar{u} \tag{A1}$$

where the following definitions have been made

$$H(c,n_0) \equiv C^{(1)}c^2 + C^{(2)}c + C^{(3)} + n_0^2 - 3n_0 + 3,$$

$$G_2(c) \equiv (C_0^{(4)} + \alpha_2)c + C_0^{(5)} + \alpha_1,$$

$$G_3(c) \equiv (C_0^{(1)}c^2 + C_0^{(2)}c + C_0^{(3)} + 3),$$

$$\chi_m(\hat{n}) \equiv \hat{n}_i\xi_{ij}^{(m)}\hat{n}_j, \quad m = 1,2,3. \tag{A2}$$

The constants appearing on the right hand sides of Eqs. (A2) are defined in Sec. II B.

Variation of $\mathcal{F}_{1D}$ with respect to ϕ_n yields

$$\frac{(\mathbf{K}^n\cdot\hat{n})^2}{2}\left\{ M_{23}(c)\frac{\partial^2\phi_n}{\partial\bar{u}^2} + M_{12}(c)\frac{\partial^2(c\phi_n)}{\partial\bar{u}^2} \right\} - \left(H(c,n_0) + 2\sum_{m\neq n}\phi_m^2 \right)\phi_n - \phi_n^3 - (2n_0-3)\prod_{m\neq n}\phi_m = 0, \quad n = 1,2,3, \tag{A3}$$

where

$$M_{12}(c) \equiv C^{(1)\prime\prime}c + \frac{C^{(2)\prime\prime}}{2},$$

$$M_{23}(c) \equiv \frac{C^{(2)\prime\prime}}{2}c + C^{(3)\prime\prime}. \tag{A4}$$

Variation of $\mathcal{F}_{1D}$ with respect to n_0 yields

$$\frac{\Gamma_{23}(c)}{4}\frac{\partial^2 n_0}{\partial\bar{u}^2} + \frac{\Gamma_{12}(c)}{4}\frac{\partial^2(cn_0)}{\partial\bar{u}^2} - \frac{1}{3}n_0^3 + \frac{3}{2}n_0^2 - \left[G_3(c) + 2\sum_m \phi_m^2 \right] n_0 + 3\sum_m \phi_m^2 - 4\phi_1\phi_2\phi_3 - [c\ln(c) + (1-c)\ln(1-c)] - G_2(c) + \mu^{eq}c + \mu_A^{eq} = 0, \tag{A5}$$

where

$$\Gamma_{23}(c) \equiv 2\chi_3(\hat{n}) + \chi_2(\hat{n})c,$$

$$\Gamma_{12}(c) \equiv \chi_2(\hat{n}) + 2\chi_1(\hat{n})c. \tag{A6}$$

Variation of $\mathcal{F}_{1D}$ with respect to c yields

$$\frac{n_0\chi_1(\hat{n})}{2}\frac{\partial^2(n_0c)}{\partial\bar{u}^2} + \sum_m (\mathbf{K}^m\cdot\hat{n})^2\phi_m\frac{\partial^2[M_{12}(c)\phi_m]}{\partial\bar{u}^2} + \frac{n_0\chi_2(\hat{n})}{4}\frac{\partial^2 n_0}{\partial\bar{u}^2} - \left(C_0^{(1)}n_0^2 + 2C^{(1)}\sum_m \phi_m^2 \right)c - n_0\ln\left(\frac{c}{1-c}\right) - \frac{C_0^{(2)}}{2}n_0^2 - (C_0^{(4)} + \alpha_2)n_0 - C^{(2)}\sum_m \phi_m^2 + \mu^{eq}n_0 = 0. \tag{A7}$$

APPENDIX B: PHASE COEXISTENCE CONDITIONS

The calculation of the surface energy requires the steady state solutions $\phi_n^*(\bar{u})$, $n_0^*(\bar{u})$, and $c^*(\bar{u})$ obtained by minimizing Eq. (6) in a planar interface geometry. The resulting differential equations for these fields require suitable boundary conditions for $c^*(\bar{u})$, $n_0^*(\bar{u})$, and $\phi_n^*(\bar{u})$ far from the interface. These far-field values are denoted $[c_s,\rho_s,\phi_{\min}(c_s,\rho_s)]$ for a solid phase and $(c_L,\rho_L,\phi{=}0)$ for a liquid phase. They are found by considering phase equilibrium between a bulk solid and liquid, described, respectively, by the free energy densities $\mathcal{G}_s$ and $\mathcal{G}_L$ in Sec. III C. A procedure for doing this is briefly outlined here.

1. General representation

Phase equilibrium between solid and liquid phases of a binary mixture are found by equating chemical potentials of species A and B (denoted μ_A^{eq}, μ_B^{eq}, respectively) and the pressures in the two phases [18,31]. Specifically,

$$\mu_A^s(\rho_A^s,\rho_B^s) = \mu_A^L(\rho_A^L,\rho_B^L) = \mu_A^{eq},$$

$$\mu_B^s(\rho_A^s,\rho_B^s) = \mu_B^L(\rho_A^L,\rho_B^L) = \mu_B^{eq},$$

$$p_s(\rho_A^s,\rho_B^s) = p_L(\rho_A^L,\rho_B^L) = p, \tag{B1}$$

where ρ_I^J denotes the average density (assumed here in [moles/m^3]) of component $I(=A,B)$ in phase $J(=s,L)$ and

$$\mu_I^J(\rho_A^J,\rho_B^J) = [\partial f_J(\rho_A^J,\rho_B^J)/\partial\rho_I^J]_{T,N} \tag{B2}$$

denotes the chemical potential (assumed here in [J/mol]) of component I in phase J, with f_J being the Gibb's free energy density [J/m^3]. Moreover,

$$p_J(\rho_A^J,\rho_B^J) = \sum_I \rho_I^J\mu_I^J(\rho_A^J,\rho_B^J) - f_J(\rho_A^J,\rho_B^J) \tag{B3}$$

denotes the pressure of phase J. The right hand sides of Eqs. (B1) are, respectively, the equilibrium chemical potentials of component A (μ_A^{eq}) and B (μ_B^{eq}) and the equilibrium pressure of the system.

Equations (B1) comprise six nonlinear equations in eight unknowns. However, the Gibb's phase rule limits to two the degrees of freedom that can be varied while maintaining phase coexistence between two alloy phases [31]. It is thus necessary to fix two of T, p, $\mu_A^{\rm eq}$, or $\mu_B^{\rm eq}$ in order to uniquely specify an equilibrium state. The natural choice here is to fix temperature (T) and pressure (p), thus reducing Eqs. (B1) six nonlinear equations in the six unknowns $(\rho_A^s, \rho_B^s, \rho_A^L, \rho_B^L, \mu_A^{\rm eq}, \mu_B^{\rm eq})$.

2. Reduced variable representation

It is useful to recast the system of Eqs. (B1) in terms of the dimensionless densities ρ_s, ρ_L, concentrations $c_{\rm s}, c_{\rm L}$, and free energies $\mathcal{G}$ used in the text. Use is made first of the mappings $\rho_B^J = \rho_J c_J$ and $\rho_A^J = (1-c_J)\rho_J$, where $J = s, L$. Moreover, instead of working with $\mu_A^{\rm eq}$ and $\mu_B^{\rm eq}$, it is convenient to define and work with the interpotential

$$\mu^{\rm eq} \equiv \mu_B^{\rm eq} - \mu_A^{\rm eq}. \tag{B4}$$

Free energy is rescaled according to $f_J(\rho_A^J, \rho_B^J)/RT\bar{\rho}_L \rightarrow \mathcal{G}_J(c_J, \rho_J)$, where R is the natural gas constant. The densities ρ_s and ρ_L are rescaled by $\bar{\rho}_L$, where $\bar{\rho}_L$ is a reference density, while pressure p is in units of $RT\bar{\rho}_L$ and $\mu^{\rm eq}$ in units of RT. In terms of these dimensionless variables Eqs. (B1) can be manipulated, after some algebra, to give

$$\frac{1}{\rho_s}\frac{\partial \mathcal{G}_s}{\partial c_s} = \mu^{\rm eq},$$

$$\frac{1}{\rho_L}\frac{\partial \mathcal{G}_L}{\partial c_L} = \mu^{\rm eq},$$

$$\frac{\mathcal{G}_L(c_L, \rho_L)}{\rho_L} - \frac{\mathcal{G}_s(c_s, \rho_s)}{\rho_s} = (c_L - c_s)\mu^{\rm eq} + \left(\frac{1}{\rho_s} - \frac{1}{\rho_L}\right)p,$$

$$\rho_L \frac{\partial \mathcal{G}_L}{\partial \rho_L} - \mathcal{G}_L = p,$$

$$\rho_s \frac{\partial \mathcal{G}_s}{\partial \rho_s} - \mathcal{G}_s = p. \tag{B5}$$

Equations (B5) can be solved to give the reduced values of $(c_s, c_L, \rho_s, \rho_L, \mu^{\rm eq})$. The reduced chemical potential $\mu_A^{\rm eq}$ is given by $\mu_A^{\rm eq} = \{p + \mathcal{G}_s(c_L, \rho_s)\}/\rho_s - c_s\mu^{\rm eq}$.

3. Equal densities

For the special case where the solid and liquid densities are equal and set to the average alloy density, i.e., $\rho_L = \rho_s = 1$, the number of unknowns reduces to $(c_s, c_L, \mu^{\rm eq})$. These three parameters are found by solving the first three of Eqs. (B5),

$$\frac{\partial \mathcal{G}_s(c_s)}{\partial c_s} = \mu^{\rm eq},$$

$$\frac{\partial \mathcal{G}_L(c_L)}{\partial c_L} = \mu^{\rm eq},$$

$$\mathcal{G}_L(c_L) - \mathcal{G}_s(c_s) = (c_L - c_s)\mu^{\rm eq}. \tag{B6}$$

Equations (B6) comprise the usual common tangent construction

[1] A. Karma and W.-J. Rappel, Phys. Rev. E **57**, 4323 (1998).
[2] B. Echebarria, R. Folch, A. Karma, and M. Plapp, Phys. Rev. E **70**, 061604 (2004).
[3] R. Folch and M. Plapp, Phys. Rev. E **72**, 011602 (2005).
[4] C. Tong, M. Greenwood, and N. Provatas, Phys. Rev. B **77**, 064112 (2008).
[5] N. Provatas, N. Goldenfeld, and J. Dantzig, Phys. Rev. Lett. **80**, 3308 (1998).
[6] N. Provatas, J. Dantzig, and N. Goldenfeld, J. Comput. Phys. **148**, 265 (1999).
[7] B. P. Athreya, N. Goldenfeld, J. A. Dantzig, M. G. Greenwood, and N. Provatas, Phys. Rev. E **76**, 056706 (2007).
[8] K. R. Elder, M. Katakowski, M. Haataja, and M. Grant, Phys. Rev. Lett. **88**, 245701 (2002).
[9] P. Stefanovic, M. Haataja, and N. Provatas, Phys. Rev. Lett. **96**, 225504 (2006).
[10] K. R. Elder, N. Provatas, J. Berry, P. Stefanovic, and M. Grant, Phys. Rev. B **75**, 064107 (2007).
[11] T. V. Ramakrishnan and M. Yussouff, Phys. Rev. B **19**, 2775 (1979).
[12] W. H. Shih, Z. Q. Wang, X. C. Zeng, and D. Stroud, Phys. Rev. A **35**, 2611 (1987).
[13] B. P. Athreya, N. Goldenfeld, and J. A. Dantzig, Phys. Rev. E **74**, 011601 (2006).
[14] K. A. Wu, A. Karma, J. J. Hoyt, and M. Asta, Phys. Rev. B **73**, 094101 (2006).
[15] K. A. Wu and A. Karma, Phys. Rev. B **76**, 184107 (2007).
[16] S. Majaniemi and N. Provatas, Phys. Rev. E **79**, 011607 (2009).
[17] K. R. Elder, Z.-F. Huang, and N. Provatas, Phys. Rev. E **81**, 011602 (2010).
[18] V. I. Kalikmanov, *Statistical Physics of Fluids* (Springer-Verlag, Berlin, 2001).
[19] R. Evans, Adv. Phys. **28**, 143 (1979).
[20] This assumes that amplitudes of each density are small relative to the average total density $\bar{\rho}_s$. This assumption can occur in some weakly first order transitions but need not be generally true.
[21] Z.-F. Huang, K. R. Elder, and N. Provatas, Phys. Rev. E **82**, 021605 (2010).
[22] K. A. Wu, A. Adland, and A. Karma, Phys. Rev. E **81**, 061601 (2010).
[23] J. W. Cahn and J. E. Hilliard, J. Chem. Phys. **28**, 258 (1958).
[24] T. Haxhimali, A. Karma, F. Gonzales, and M. Rappaz, Nature

Mater. **5**, 660 (2006).
[25] C. A. Becker, D. Olmsted, M. Asta, J. J. Hoyt, and S. M. Foiles, Phys. Rev. Lett. **98**, 125701 (2007).
[26] M. Amini and B. B. Laird, Phys. Rev. B **78**, 144112 (2008).
[27] A. Passerone and N. Eustathopoulos, Acta Metall. **30**, 1349 (1982).
[28] W. A. Miller and G. A. Chadwick, Proc. R. Soc. London, Ser. A **312**, 257 (1969).
[29] K. K. Mon, S. Wansleben, D. P. Landau, and K. Binder, Phys. Rev. Lett. **60**, 708 (1988).
[30] J. J. Hoyt, private communication.
[31] L. Landau and E. Lifsitz, *Statistical Physics*, 3rd ed. (Butterworth-Heinemann, Oxford, 1987).